HELICAL ANTENNAS

The helix antenna has a long and fascinating history. It was discovered in 1946 by John Kraus. Since then, new variations have continued to arise, even up to the present day. The discovery itself is a very interesting story, which is told in John Kraus's book *Antennas* (1). It all started with an afternoon lecture at Ohio State University. John Kraus listened as the speaker described the wave-guiding helix used in traveling-wave tubes; he wondered if this interesting helix could be used as an antenna and, after the talk, he asked the well-known lecturer. The speaker replied emphatically, "No, I've tried it and it doesn't work." That very evening, John Kraus went down to his basement, wound a seven-turn helical coil one wavelength in circumference and fed it by means of a coaxial line and ground plane [Fig. 1(a)]. He found that it produced a sharp beam of circularly polarized radiation off the open end of the helix. So the helix antenna was born, despite the advice of experts.

Helical Curves

The helix was well-known in ancient Greece. Geminus described it in the first century B.C. and there are references to earlier work on the helix. The *cylindrical helix* may be defined by considering a right circular cylinder of radius a, whose axis is the z axis. Using a right-handed cylindrical coordinate system (r, ϕ, z) the equations of the helix are

$$x = a\cos\phi \quad y = a\sin\phi \quad z = a\phi\tan\alpha \tag{1}$$

where α is the pitch angle of the helix and $2a$ is the diameter. The lines of the cylinder parallel to the z axis, that is, the lines $(r = a, \phi = \phi_0)$ are considered to be the generators of the cylinder. The cylinder is generated by rotating any generator about the z axis. The helix cuts the generators at a *constant angle* $(\pi/2) - \alpha$. It also projects as a sine curve on any plane parallel to the axis, for example, any plane that includes the axis.

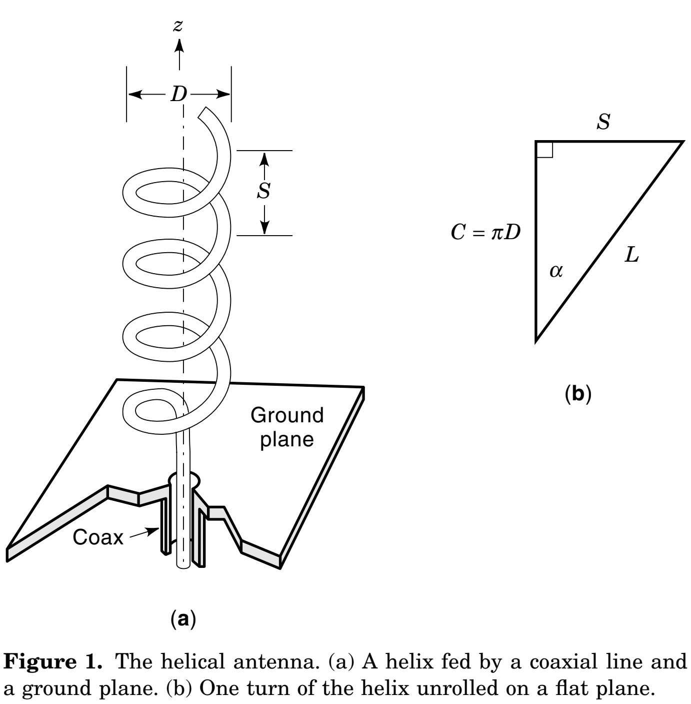

Figure 1. The helical antenna. (a) A helix fed by a coaxial line and a ground plane. (b) One turn of the helix unrolled on a flat plane.

Figure 1(a) shows the wire helix antenna. Parameters are defined as follows:

D is the diameter of helix, which is equal to $2a$.
C is the circumference.
S is the spacing between turns.
α is the pitch angle.
L is the length of one turn.
N is the number of turns.

C_λ, S_λ, and L_λ represent the respective distances in wavelengths such that $C_\lambda = C/\lambda$, and so on. When one turn of the helix is unrolled on a flat plane, the relationships between the spacing S, circumference C, and turn length L and pitch angle α can be obtained from the triangle shown in Fig. 1(b) as follows:

$$S = C\tan\alpha \quad \alpha = \tan^{-1}\frac{S}{C} \quad L = \sqrt{C^2 + S^2} \tag{2}$$

Thus we need only *three* independent parameters C, α, N to describe a helix. Note that when $\alpha = 0°$, $S = 0$, and the helix reduces to a planar loop. When $\alpha = 90°$, $C = 0$ and the helix becomes a straight line.

The round-wire helix such as Kraus first built consists of a round wire of a radius whose axis is the helix curve of Eq. (1). The tape helix is a conducting tape of width w, which is wound around a cylinder or a thin cylindrical tube. Its centerline is the helix of Eq. (1). A single-wire helix is called the *monofilar helix.* The double, or *bifilar,* helix is constructed by adding an additional member, which is formed by replacing ϕ with $\phi - \pi$ everywhere in Eq. (1). The *quadrifilar* helix antenna is formed by adding three members; ϕ in Eq. (1) is replaced with $\phi - (\pi/2)$, π, $(3\pi/2)$. A left-handed helix can be formed by using a left-handed coordinate system, or by replacing ϕ in Eq. (1) with $2\pi - \phi$. Figure 1(a) shows a right-handed helix. There are other helical curves. The *conical helix* lies on the surface of a cone and cuts the radial lines of the cone, the generators, at a constant angle. The *spherical helix* lies on the surface of the sphere and cuts the generators, for example, the longitude lines, at a constant angle.

There are many striking examples of the helix in nature, from some of the smallest to some of the largest objects. Most important of all is the deoxyribonucleic acid (DNA) molecule, which is a double helix. The marks on a snail of the family Helicidae resemble a spherical helix. The human ear has a prominent helical ridge. The Heliconia is a family of herbs with a helical shape. The helictite is similar to a stalagtite. Some trees have helical bark. Finally, we have the largest of the nebulae, the Helix Nebula. In addition, we see many manmade forms of the helix around us, including automobile springs, spiral staircases, inductance coils, transformer coils, parking lot ramps, automobile antenna coils, and finally, the lowly screw, which is a combination of conical and cylindrical helices.

MONOFILAR HELICAL ANTENNA

We first consider the characteristics of a monofilar, or unifilar, helical antenna. In this section we simply call it a helical

J. Webster (ed.), *Wiley Encyclopedia of Electrical and Electronics Engineering.*

antenna, implying that it is a *monofilar* helix. The helix commonly operates in two different modes, the normal mode and the axial mode depending on the electrical size of the helix. When the dimensions of the helix are small compared with a wavelength ($D \ll \lambda$, $NS \ll \lambda$), the maximum radiation is normal (or perpendicular) to the helix axis. This condition is called the *normal mode.* When the helix circumference is on the order of one wavelength, the maximum radiation is along the helix axis. Thus, this type of operation is called the *axial mode.* The axial mode helix is a broadband antenna. The radiation from this axial mode helix is close to circular polarization along the axis. There is also a *backfire* mode which is discussed in a later section.

Normal Mode Helix

Let's consider a helix with its axis along the z axis, centered at the origin [Fig. 2(a)]. The geometry of the helix reduces to a loop when the pitch angle α approaches zero and to a straight wire when it approaches 90°. Since the limiting geometries of the helix are a loop and a dipole, the far field radiated by a small helix can be described by the radiation fields of a small loop and a short dipole when dimensions are small compared to a wavelength. The analysis of a small short helix is facilitated by assuming that the helix consists of a number of small loops and short dipoles connected in series as in Fig. 2(b). The diameter of the loops is the same as the helix diameter (D) and the length of the dipoles is approximately the same as the spacing (S) between turns of the helix. Because the helix is small and short, the current distribution is assumed to be *uniform* in magnitude and phase over the entire length of the helix. For the same reason, the far-field pattern will be independent of the number of turns and thus can be obtained by considering the pattern of a single-turn helix which consists of a single small loop of diameter D and one short dipole of length S.

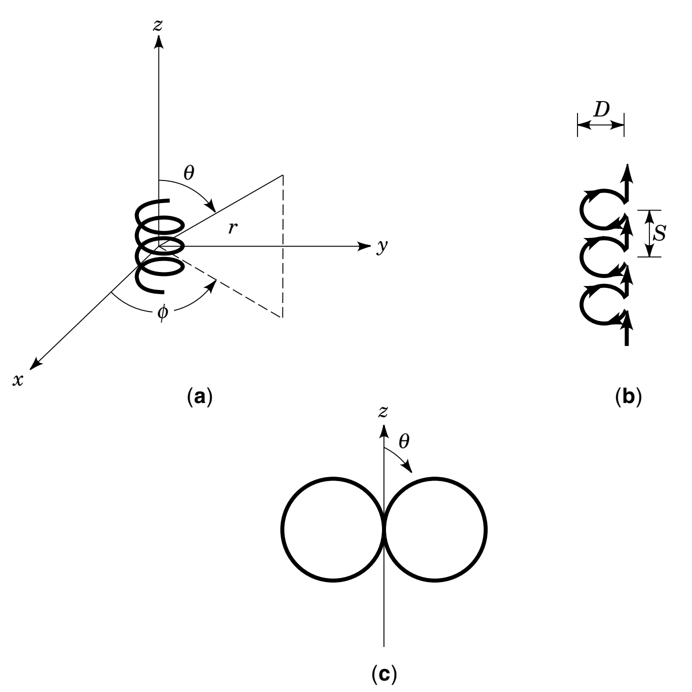

Figure 2. The normal mode helix. (a) Coordinate system. (b) Loop and dipole model. (c) Beam pattern.

Assume that the complex amplitude of current is I and the angular frequency is ω. The radiation electric field of the small loop of diameter D has only an E_ϕ component, given by

$$E_\phi = \eta k^2 IA \frac{e^{-jkr}}{4\pi r} \sin\theta \tag{3}$$

where $A = \pi D^2/4$ is the area of the loop, $k = \omega\sqrt{\mu\epsilon}$ the propagation constant, and $\eta = \sqrt{\mu/\epsilon}$ the intrinsic impedance. The far field of the short dipole, or the Hertzian dipole of length S, has only an E_θ component, given by

$$E_\theta = j\omega\mu IS \frac{e^{-jkr}}{4\pi r} \sin\theta \tag{4}$$

The total radiation field for one turn is then given by

$$\mathbf{E} = \mathbf{a}_\theta E_\theta + \mathbf{a}_\phi E_\phi = \{\mathbf{a}_\theta j\omega\mu S + \mathbf{a}_\phi \eta k^2 A\} I \frac{e^{-jkr}}{4\pi r} \sin\theta \tag{5}$$

The normalized radiation field pattern $f(\theta)$ of the normal mode helix is

$$f(\theta) = \sin\theta \tag{6}$$

which is the same as that of the Hertzian dipole and the small loop and is shown in Fig. 2(c). The field is zero along the axis (in the end-fire direction) and is maximum in the xy plane ($\theta = 90°$), which is normal to the helix axis.

Because E_θ and E_ϕ are 90° out-of-phase, as shown in Eqs. (3) and (4), the radiated wave is elliptically polarized. The axial ratio (AR) of the polarization ellipse of the far field is obtained by dividing the magnitude of Eq. (4) by that of Eq. (3):

$$\mathrm{AR} = \frac{|E_\theta|}{|E_\phi|} = \frac{\omega\mu S}{\eta k \dfrac{2\pi}{\lambda} A} = \frac{S\lambda}{2\pi A} = \frac{2S\lambda}{(\pi D)^2} \tag{7}$$

where we have used $k = 2\pi/\lambda$, $\eta k = \omega\mu$. Because E_θ and E_ϕ are 90° out-of-phase, the polarization ellipse becomes a circle when $|E_\phi| = |E_\phi|$, indicating circular polarization. Setting AR = 1 yields

$$C = \pi D = \sqrt{2S\lambda} \quad \text{or} \quad C_\lambda = \sqrt{2S_\lambda} \tag{8}$$

Under this condition the radiation field is circularly polarized in all directions except of course along the axis where the radiation is zero. The polarization ellipse of the radiation from a helix of constant turn-length (L) changes progressively as the pitch angle α is varied. When $\alpha = \tan^{-1}(S/C) = 0$ (the helix reduces to a loop), AR = 0, $E_\theta = 0$, $\mathbf{E} = \mathbf{a}_\phi E_\phi$; thus the wave is linearly polarized with horizontal (or perpendicular) polarization. As α increases, the polarization becomes elliptical with the major axis of the ellipse being horizontal. When α reaches a value such that condition (8) is satisfied, AR = 1, and the polarization is circular. With the help of Eq. (2), the condition (8) leads to the following value of α:

$$\alpha_{\mathrm{CP}} = \sin^{-1}\left[\frac{-1 + \sqrt{1 + L_\lambda^2}}{L_\lambda}\right] \tag{9}$$

As α increases further, the polarization again becomes elliptical with the major axis being vertical. Finally, when $\alpha = 90°$ (the helix reduces to a dipole), AR $= \infty$, $E_\phi = 0$, $\mathbf{E} = \mathbf{a}_\theta E_\theta$; thus the polarization is linear with vertical (or parallel) polarization. For small pitch angles ($\alpha \ll 1$), Eq. (9) is simplified to

$$\alpha_{\mathrm{CP}} = C_\lambda/2 \tag{10}$$

where α_{CP} is in radians. For small pitch angles, circular polarization can occur at frequencies such that the circumference is very small compared to a wavelength ($C_\lambda \ll 1$).

From Eqs. (3) and (4), we note that the loop field E_ϕ and the dipole field E_θ, respectively, are proportional to the second and first powers of frequency. Correspondingly, radiation resistance of loop and dipole are proportional to the fourth and second powers, respectively. Thus, as frequency decreases, the dipole radiation predominates and the beam pattern is *linearly* polarized. In this linearly polarized frequency range, the normal mode helix has some interesting properties. Its beam pattern is essentially that associated with the dipoles, that is, a monopole of length NS above a ground plane. Its impedance, however, is significantly affected by the loops.

The normal mode helix is limited by its size. It has the same restrictions and limitations that apply to any electrically small antenna. But within those restrictions, it has certain advantages over a dipole antenna of the same height. These include a lower frequency for resonance and a larger radiation resistance, both because of the longer path of the helical structure. While the dipole may require additional impedance-matching circuits to achieve resonance, the helix is resonant without supplementary matching elements. Another advantage over the dipole is that the helix is flexible and more resilient. The higher radiation resistance, resonant characteristic, and flexibility make the normal mode helix suitable for small antennas used in mobile communications.

Axial Mode Helix

A very useful mode of operation for the helical antenna is the axial or endfire mode. In this mode the radiation pattern has a single main beam along the axis of the helix ($+z$ direction), that is, it is an endfire antenna. Experiments have shown that the axial mode occurs when the circumference of the helix is approximately one wavelength and when the helix has several turns. A primary component of current on the helix is a wave traveling outward from the feed along the wire at approximately the speed of light and the radiation is a beam off the end of the helix. Because the electric field vector rotates around in a circular fashion as does the current on the helix, we expect that the radiation field is circularly polarized along the helix axis. One very important feature of the axial mode helical antenna is its *broadband* character. As a rule of thumb, the approximate bandwidth for the axial mode is given as follows (2):

$$\frac{3}{4} < C_\lambda < \frac{4}{3} \tag{11}$$

The bandwidth ratio, the ratio of the upper and lower frequencies is $4/3 \div 3/4$ or 1.78, which is close to a 2 : 1 bandwidth. The helix is usually fed axially or peripherally with the inner conductor of the coaxial line connected to the helix and the outer conductor attached to the ground plane. The ground plane can be made from either solid metal or wire mesh.

Analysis of Radiation Pattern. The axial mode helix has a circumference of approximately one wavelength, so the current distribution would not be uniform, and we assume that there is an outgoing current wave, traveling along the helical conductor at phase velocity $v = pc$ (p is the phase velocity relative to the speed of light c in free space). Then

$$I(\ell) = I_0 e^{-j\beta\ell} \tag{12}$$

where ℓ is the distance measured along the helix from the beginning of the turn closest to the ground plane, I_0 the input current, $\beta = k/p$ the phase constant of the current wave. When the total length of one turn is approximately a wavelength, the current distribution in Eq. (12) has opposite phase (180° out-of-phase) on opposite sides of a turn, because they are separated by about a half-wavelength. Also the helical coil physically reverses current direction for opposite points. Thus the currents at opposite points of a turn are essentially in phase, giving rise to reinforcement in the far field along the helix axis. We can find the radiation pattern by using the principle of pattern multiplication because a helix with uniform cross section can be considered as an array of N identical elements (or turns). We have a uniformly excited, equally spaced array with spacing S, so the total pattern is the product of the pattern for one turn (the element pattern) and the pattern for an array of N isotropic point sources (an array factor). When the helix is long (say, $NS > \lambda$), the array factor is much sharper than the element pattern and hence determines the shape of the total far-field pattern.

Array Factor. The array factor (AF) of a uniformly excited, equally spaced, linear array of N elements is given by

$$\mathrm{AF} = \frac{\sin[(N/2)\Psi]}{N\sin(\Psi/2)} \tag{13}$$

and

$$\Psi = kS\cos\theta + \delta \tag{14}$$

where θ is an angle measured from the array axis (z axis) and δ is the phase shift between adjacent elements. Explaining the phase relationships of the axial mode helix is difficult. Begin by finding the phase shift δ required for endfire operation, because we know that the radiation is endfire. For *ordinary endfire,* we find the conditions such that Ψ is zero at $\theta = 0°$:

$$\delta = -kS - 2m\pi \quad m \text{ is an integer} \tag{15}$$

where the term $(-2m\pi)$ reflects the basic ambiguity of phase. Next we find conditions for *increased directivity Hansen–Woodyard (H–W)* (3) *endfire,* since this is an optimum form of endfire:

$$\begin{aligned}\delta &= -kS - 2m\pi - \pi/N \\ &= -2\pi - (kS + \pi/N) \quad m = 1\end{aligned} \tag{16}$$

To be more accurate, ther term π/N should be replaced by $2.94/N$ (3). However, the choice of π/N hardly changes the radiation field (4) and is convenient for expressing other quantities. We have tried the arbitrary choice ($m = 1$), because this term -2π corresponds roughly to one turn of the circumference at midband ($C_\lambda = 1$). Later it will be clear that other choices are not possible solutions. Experiments show (1,5) that the phase shift δ obtained is close to that of Eq. (16) at midband ($C_\lambda = 1$). How does this happen? We have already pointed out that the term (-2π) corresponds roughly to one turn of the circumference. In addition, the length around one turn of the helix is greater than a wavelength ($L_\lambda > 1$) at midband. More importantly, the velocity of travel is less than that of light ($p \approx 0.9$) at midband (5). These two additional contributions account for the minor terms $-(kS + \pi/N)$. Thus the phase at midband is explained. However, the experimental data for δ tracks Eq. (16) fairly well over the entire bandwidth of the axial mode. How is this possible? We cannot alter our choice of m; one choice must work for the entire frequency range. And if p remained constant, Eq. (16) could not be satisfied over the entire band. Fortunately, p does vary quite a bit (from 0.73 to 0.97) over the axial mode frequency range; the result is that H–W endfire described by Eq. (16) is tracked quite well over most of the band, falling off a little toward the high end. All in all, this is quite a remarkable story. The phase, so to speak, *locks in* to H–W endfire over the bandwidth of almost 2:1. When first reported by Kraus, this was called an *anomalous* phase progression. It still continues to mystify succeeding generations.

To summarize, the phase progression along the helix wire is relatively simple; it corresponds roughly to that of the speed of light along the wire. The phase progression in z, which determines the phase difference δ between turns, follows the phase progression of the wire. Taking into account the phase ambiguity ($2m\pi$), we see that H–W endfire is obtained at midband. The relative phase velocity p then changes with frequency just enough to maintain the H–W endfire. Another point worth noting is that we have not discussed backfire ($\theta = 180°$) radiation. It does, in fact, occur along with the axial mode but is usually suppressed by the ground plane. It will return, to our advantage, with the multifilar helix.

Assuming, then, the validity of Eq. (16),

$$\beta = -\frac{\delta}{L} = \frac{1}{L}\left[kS + 2\pi\left(1 + \frac{1}{2N}\right)\right] = \frac{2\pi}{L}\left(\frac{S}{\lambda} + \frac{2N+1}{2N}\right) \quad (17)$$

$$p = \frac{k}{\beta} = \frac{L_\lambda}{S_\lambda + (2N+1)/2N} \quad (18)$$

Using p as obtained from Eq. (18) to calculate the array factor yields patterns in good agreement with measured patterns. The p value calculated from Eq. (18) also is in closer agreement with measured values of p (1). Therefore, it appears that the Hansen–Woodyard increased directivity condition is a good approximation for helices radiating in the axial mode. For a typical case where $C = \lambda$, $\alpha = 14°$, $N = 10$, we find from Eq. (18) that $S = C \tan \alpha = 0.249\lambda$, $L = 1.031\lambda$, and $p = 0.79$. Thus the traveling current wave has a phase velocity less than that of free space. Finally, substituting Eq. (16) into Eq. (14) yields

$$\Psi = kS(\cos\theta - 1) - \left(2\pi + \frac{\pi}{N}\right) \quad (19)$$

Equations (13) and (19) provide the complete normalized array pattern of the axial mode helical antenna. For the element pattern we will need an analysis of the radiation from a circular loop, which is covered in the next section.

Circular Loop Radiation. In this section we consider the radiation from a circular loop carrying a current $I(\phi)$. The result is useful in understanding the operation of the helix in both the mono- and multifilar forms. In addition, it will yield an approximate element factor for a single turn of the helix. The loop of radius a is centered at the origin and lies in the xy plane. The current distribution $I(\phi)$ may be represented in terms of a complex Fourier series representation:

$$I(\phi) = \sum_{n=-\infty}^{\infty} I_n e^{jn\phi} \quad (20)$$

Consider the typical term $I_n e^{jn\phi}$ of the current distribution $I(\phi)$. First we evaluate components $A_{\phi n}$, $A_{\theta n}$ of the far-field magnetic vector potential as follows. Directions ϕ, θ are associated with the field point rather than the source point.

$$A_{\phi n} = \frac{e^{-jkr}}{4\pi r}\int_0^{2\pi} I_n e^{jn\phi'} \cos(\phi - \phi') e^{jka \sin\theta \cos(\phi-\phi')} a\, d\phi' \quad (21)$$

$$A_{\theta n} = \frac{e^{-jkr}}{4\pi r}\int_0^{2\pi} I_n e^{jn\phi'} [-\sin(\phi' - \phi)] \cos\theta\, e^{jka \sin\theta \cos(\phi-\phi')} a\, d\phi' \quad (22)$$

To evaluate A_ϕ, we introduce the change of variables $\Psi = \phi' - \phi$ and change limits to obtain

$$A_{\phi n} = \frac{e^{jn\phi} e^{-jkr} I_n a}{4\pi r}\int_0^{2\pi} e^{jn\Psi}\left(\frac{e^{j\Psi} + e^{-j\Psi}}{2}\right) e^{j(ka \sin\theta)\cos\Psi} d\Psi$$

Next, we use the following integral expression for the Bessel function of the first kind $J_m(x)$:

$$\int_0^{2\pi} e^{jx\cos\theta} e^{jm\theta} d\theta = 2\pi j^m J_m(x)$$

A_ϕ is then evaluated directly to obtain

$$A_{\phi n} = \frac{e^{jn\phi}(I_n a) e^{-jkr} j^{n+1}}{4r}[J_{n+1}(ka\sin\theta) - J_{n-1}(ka\sin\theta)] \quad (23)$$

$$E_{\phi n} = -j\omega\mu A_{\phi n} \quad (24)$$

Using similar methods, we obtain the following evaluation of A_θ.

$$A_{\theta n} = \frac{e^{jn\phi}(I_n a) e^{-jkr} j^{n+1}(j\cos\theta)}{4r}[J_{n+1}(ka\sin\theta) + J_{n-1}(ka\sin\theta)] \quad (25)$$

$$E_{\theta n} = -j\omega\mu A_{\theta n} \quad (26)$$

The total fields may of course be obtained by adding contributions of all Fourier modes.

Now let's evaluate the far fields along the z axis ($\theta = 0°$, $180°$) for each of the separate Fourier modes. We note that $J_n(0) = 0$ ($n \neq 0$) and $J_0(0) = 1$. Evaluating the cases $n = \pm 1$, we find that, along the z axis,

$$\frac{E_\phi}{E_\theta} = \pm j \tag{27}$$

In other words, the modes $n = \pm 1$ representing traveling waves yield circular polarization along the z axis. Note that all other traveling-wave modes yield a null on axis. Of all the Fourier modes, only $n = \pm 1$ radiate in the forward endfire or backfire directions. For the helix, we define forward or backward radiation as radiation away from or toward the feed point, respectively.

This result can also be seen by considering currents around the loop for various modes. For $n = \pm 1$, each current element is matched by its opposite across the loop that is in the same direction such as to add along the z axis and to rotate polarization as time progresses. All of the other modes cancel along the axis. For even modes, each element is cancelled by its opposite across the loop. For odd modes, a group of elements will cancel. For the general odd case n, any group of n elements each separated by $180°/n$ yields zero contribution. For $n = 5$, for example, any group of five elements each separated by 36° yields zero contribution.

Any currents on the cylindrical surface may be resolved into ϕ- and z-directed currents. The z-directed currents do not radiate along the axis. Thus, for currents of any direction, only the $n = \pm 1$ Fourier modes can contribute to endfire or backfire. These results will be useful when considering multifilar helices.

The above discussion makes it easier to understand the operation of the helical antenna. At low frequencies the zeroth mode ($n = 0$) is strongly excited, because there is little variation of phase around the cylinder on one turn. In addition, the impedance of the higher modes is highly reactive. As frequency increases and C_λ approaches unity, we have one complete cycle around the cylinder on one turn, and we expect the $e^{-j\phi}$ mode to be excited for a right-hand helix. The phase velocity of the helix is lower than that associated with the speed of light and the impedance of the mode $n = -1$ is reasonable, and so the axial mode begins at approximately $C_\lambda = 0.75$. Similarly, as frequency increases we expect the mode $n = -2$ to appear; this mode would produce beam pattern deterioration. The axial mode continues until about $C_\lambda = 1.33$.

Element Pattern of the Axial Mode Helix. For the element pattern of one turn of the helix, the current distribution is assumed to be

$$I(\phi') = I_0 e^{-j\beta\ell} = I_0 e^{-j\beta a\phi'} \tag{28}$$

where $\beta = k/p$, $a = D/2$ and ϕ' is the angle measured from the x axis. For accurate analysis of the element pattern, Eq. (28) should be used to calculate the radiation integral. However, when the helix with several turns operates in the axial mode ($C_\lambda \approx 1$), the array factor dominates the endfire beam pattern and the element pattern provides minor corrections. Thus it suffices to consider the radiation field of a planar loop with $C_\lambda = 1$, instead of a three-dimensional one-turn helix. If we also assume that $p \approx 1$, then

$$I(\phi') \approx I_0 e^{-jka\phi'} = I_0 e^{-j(2\pi/\lambda)a\phi'} \approx I_0 e^{-j\phi'} \tag{29}$$

Using the simple form of the current distribution in Eq. (29), we can easily calculate the radiation fields for the element pattern from Eqs. (23)–(26) for $C_\lambda = 1$ ($n = -1$):

$$E_\phi(\theta,\phi) = C(r)[J_0(\sin\theta) + J_2(\sin\theta)]\, e^{-j\phi} \tag{30}$$

$$E_\theta(\theta,\phi) = C(r)[J_0(\sin\theta) - J_2(\sin\theta)](j\cos\theta)\, e^{-j\phi} \tag{31}$$

where $C(r)$ gives the r dependence of the fields. Note that $ka = 1$ when $C_\lambda = 1$. If we plot the radiation patterns of $|E_\theta|$ and $|E_\phi|$ using Eqs. (30) and (31) we obtain a figure-eight pattern for E_θ with a null at 90°, and a nearly omnidirectional pattern for E_ϕ (6). From the plot, it is interesting to note that the normalized E_θ can be approximated by $\cos\theta$. We also observe that E_θ and E_ϕ are 90° out of phase. In particular, when $\theta = 0°$, $|E_\theta| = |E_\phi|$, thus the radiation field is *circularly polarized* in the endfire direction. As one departs from $\theta = 0°$, E_θ decreases more rapidly than does E_ϕ, so the polarization becomes elliptical. Finally, it should be noted that Kraus (1) has analyzed the element pattern, by using a single turn of a three-dimensional helix with uniform traveling wave current.

Beam Patterns. The complete total far-field pattern is given by the product of the array factor shown by Eq. (13) and the element pattern in Eq. (30) or Eq. (31). However, the array pattern is much sharper than the element patterns. Thus the total E_θ and E_ϕ patterns are nearly the same, in spite of the difference in the single-turn patterns. The main lobes of the E_θ and E_ϕ patterns are very similar to the array pattern. Therefore, for long helices ($NS > \lambda$), a calculation of only the array factor is sufficient for an approximate pattern of any field component of the helix.

The measured patterns of a six-turn helix with $\alpha = 14°$ as a function of frequency are presented in Fig. 3. Patterns are shown over a range of circumferences from approximately 0.66λ to 1.35λ. The solid patterns are for the horizontally polarized component (E_ϕ) and the dashed for the vertically polarized (E_θ). Both are adjusted to the same maximum. We observe that the endfire beam patterns are preserved over the range of $0.73 < C_\lambda < 1.22$, indicating that the axial mode helix is a broadband antenna.

Important Parameters. Four important parameters for practical design of an axial mode helical antenna are beamwidth (BW), gain or directivity, input impedance, and axial ratio (AR). They are all functions of the number of turns, the turn spacing (or pitch angle), and the frequency. For a given number of turns, the behavior of the BW, gain, impedance, and AR determines the useful bandwidth. The nominal center frequency of this bandwidth corresponds to a helix circumference of about 1λ.

Beam Width. Based on a large number of measurements King and Wong (7) give the following quasiempirical formula for the beamwidths:

$$\text{HPBW (half-power beam width)} = \frac{K_B}{C_\lambda\sqrt{NS_\lambda}}\ \text{[degrees]} \tag{32}$$

where K_B varies from 61 to 70, for $3/4 < C_\lambda < 4/3$, $12° < \alpha < 15°$, and $8.6 < N < 10$. Note that as N increases the beamwidth decreases. Figure 4(a) shows measured HPBW of a six-turn, 14° axial-mode helix as a function of the normalized cir-

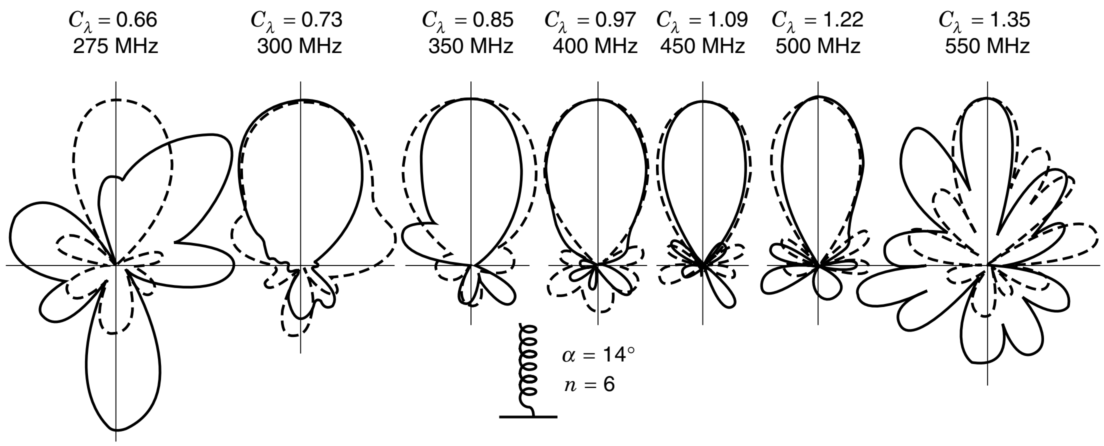

Figure 3. Measured beam patterns of the monofilar axial mode helix. From Kraus (1). © 1988 by McGraw-Hill, Inc. Reprinted with permission of the McGraw-Hill Companies.

cumference (C_λ). We observe that HPBW changes slowly over the range of approximately $0.7 < C_\lambda < 1.25$.

Gain. The gain of the axial mode helix can be approximately obtained (8) by

$$G = K_G C_\lambda^2 N S_\lambda \tag{33}$$

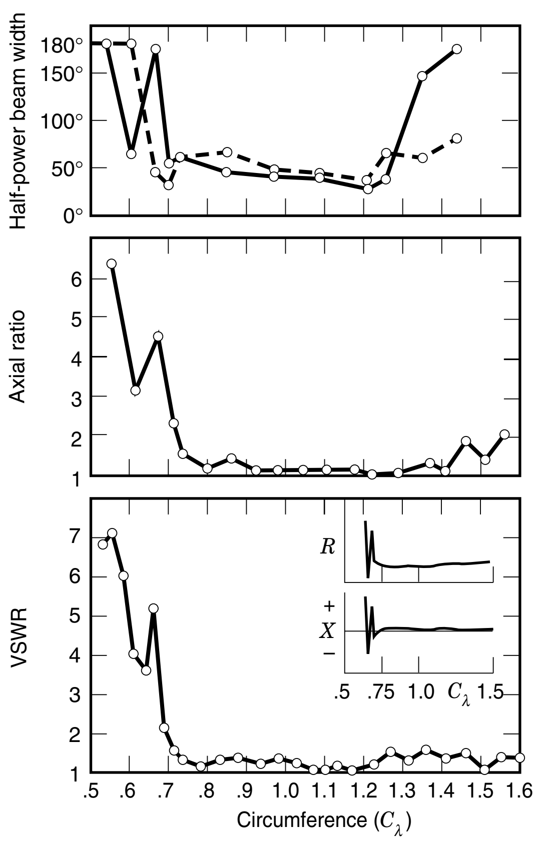

Figure 4. Measured performance of the monofilar axial mode helix. (a) Beamwidth. (b) Axial ratio. (c) VSWR. From Kraus (1). © 1988 by McGraw-Hill, Inc. Reprinted with permission of the McGraw-Hill Companies.

where K_G is the gain factor which depends on the design parameters. King and Wong (7) report that K_G varies from 4.2 to 7.7. Experiments show that the gain is peak when C is slightly larger than 1λ.

Axial Ratio. We have shown from the approximate analysis described in a previous section that the radiation field is circularly polarized in the mainbeam direction ($\theta = 0°$), implying AR = 1. With a more accurate analysis including the effect of relative phase velocity for increased directivity, Kraus (1) obtains the axial ratio along the helix axis as follows:

$$\mathrm{AR} = \frac{2N+1}{2N} \quad (\theta = 0^\circ) \tag{34}$$

If N is large, the axial ratio approaches unity and the polarization is nearly circular. For example, for a six-turn helix, AR = 13/12 = 1.08 according to Eq. (34). This axial ratio is independent of frequency or circumference. In Fig. 4(b), the measured values of the axial ratio for the six-turn, 14° axial-mode helix are plotted as a function of the circumference (C_λ). We observe that AR is nearly 1 over the range of about $0.73 < C_\lambda < 1.4$. The sense of circular polarization is determined by the sense of the helix windings.

Input Impedance. The input impedance of the axial mode helical antenna is nearly purely resistive. The empirical formulas for the input resistance are given (1) by

$$R_{\text{in}} = 140 C_\lambda \tag{35}$$

within 20% for the case of axial feed, and

$$R_{\text{in}} = 150/\sqrt{C_\lambda} \tag{36}$$

within 10% for the case of peripheral feed. Both relations are valid when $0.8 \le C_\lambda \le 1.2$, $12° \le \alpha \le 14°$ and $N \ge 4$. With a suitable matching section, R_{in} can be made any desired value from 50Ω to 150Ω. In the inset of Fig. 4(c), trends of input resistance R and reactance X are shown as a function of the relative frequency or circumference. Note that R is relatively constant and X is very small for $0.7 < C_\lambda < 1.5$. Figure 4(c) also shows the voltage standing wave ratio (VSWR) measured on a 53Ω coaxial line. We observe that the VSWR nearly remains constant (approximately 1), and equivalently the input impedance of the helix remains unchanged, over the range of about $0.7 < C_\lambda < 1.6$.

Broadband Characteristics. Considering all the characteristics of beam pattern, input impedance, and polarization as a function of circumference, we find that the performance of the axial mode helix is satisfactory over the range of about $0.75 < C_\lambda < 1.25$ within the restrictions given on α and N. Thus the bandwidth, defined by the ratio of upper and lower frequencies, is almost an octave. The broadband characteristics of the helix can be explained by the natural adjustment of the phase velocity. As the helix size C_λ, or equivalently the frequency, varies over rather wide range, the phase velocity adjusts itself automatically such that the fields from each turn add nearly in phase in the axial direction.

Variations and Applications of the Helical Antenna

A slight taper on the end of the helix (9,10) reduces the axial ratio at the expense of a slight reduction in gain. Axial ratio is improved both on and off axis. A taper is also used at the input to improve impedance characteristics. A circular-cavity backing is sometimes used to reduce the back radiation and increase the forward gain. Dielectric-tube support has been used with the helix antenna. This lowers the frequency for the onset of axial-mode operation and has an effect on the terminal impedance. A solid dielectric core has also been used with the helix (the polyrod helix). A helix with an inner concentric metal core has been used as a TV transmitter (11). The antenna utilizes higher order Fourier modes such as $e^{\pm j2\phi}$, $e^{\pm j5\phi}$ which radiate sidefire rather than endfire. This is particularly useful with towers and masts whose circumference is much larger than a wavelength. An array of helices is stacked along the mast to produce the required beam pattern. The helical antenna has often been used as an element in various types of arrays. Large planar arrays of helices have been used in radio astronomy (12). An array of axial-mode helices has been used for global positioning system (GPS) satellite transmitters (1). Helices are also used as feeds for parabolic dishes. Applications of the helix are legion.

MULTIFILAR HELIX ANTENNAS

The helical antenna described in the preceding section may be termed the monofilar helical antenna. It is constructed from a single wire, or tape, and fed from a single source. In this section we consider the multifilar helix antenna, which consists of a number of wires or tapes, each of which may be fed from a separate source. The wires may be interleaved as shown in Fig. 5(a) for the quadrifilar helix. The excitations in all cases discussed is of the form $e^{\pm j\phi}$. Other excitations are certainly possible but have not been thoroughly studied. Many different forms of the multifilar helix have been used, including bifilar, quadrifilar, and octofilar helices. There are two distinct classes of multifilar helices which have been used, namely, the broadband forward-fire axial mode multifilar helix and the narrowband backfire multifilar helix. For both, the quadrifilar helix has been widely studied and used.

We have already discussed the Fourier modes due to a loop of circumferential current. The rigorous consideration of the entire geometry of the helix yields modes with the same ϕ dependence but yields the phase progression in z as well. Samuel Sensiper (13) carried out this rigorous analysis to determine the real propagation constants of the normal and axial modes. He also determined some of the characteristics of the multifilar helix. Later, Paul Klock (14) found an additional mode with a complex propagation constant. This mode starts with backfire then splits and scans forward as a conical beam as frequency increases. It operates simultaneously with the axial mode but is usually suppressed by the ground plane. Early experimenters of the multifilar helix showed some improvements over the monofilar helix but did not always recognize that larger bandwidth could be obtained nor how to obtain it, as explained in the following section.

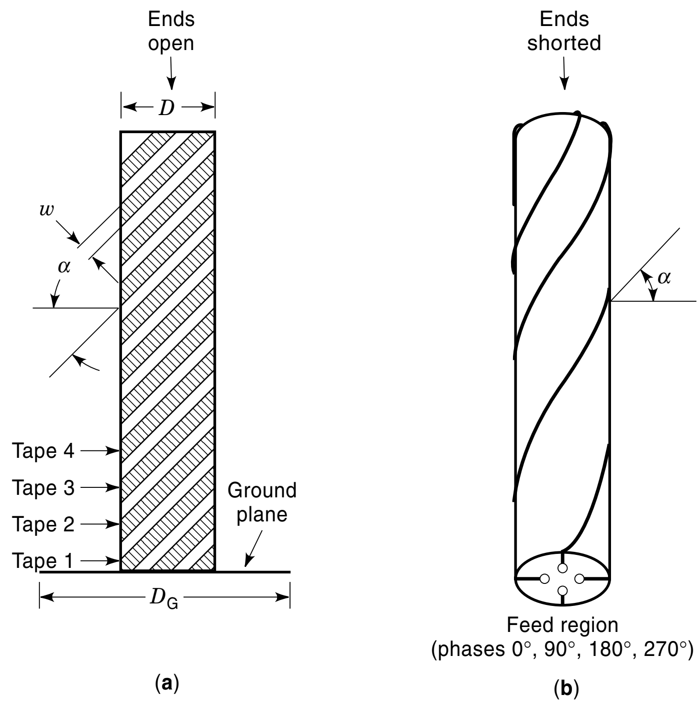

Figure 5. Quadrifilar helical antenna. (a) Endfire. (b) Backfire.

The Axial Mode Quadrifilar Helix

Gerst and Worden (15) invented the broadband axial mode multifilar helix. He pointed out that the frequency range of the axial mode could be extended by (1) adding more wires, (2) using $e^{-j\phi}$ excitation to maintain that mode and suppress others, and (3) increasing the pitch angle α. The technique is readily understood by considering the bifilar helix. First, the two wires are fed 180° out of phase. Consider a cross section perpendicular to the helix axis. We find, in any cross section, two wires 180° apart in space and phase. Only the odd Fourier modes ($e^{jn\phi}$, n odd) are excited. The mode $e^{-j2\phi}$, which may be a culprit in the pattern breakup of the monofilar helix, is suppressed. The mode $e^{-j3\phi}$ is not suppressed and the bandwidth for the axial mode approaches 3:1. A pitch angle of about 25–30° is required. Now consider the quadrifilar helix. A cross section through the right-hand helix of Fig. 5(a) displays four wires symmetrically arranged around the periphery, with phases 0, −90, −180, and −270°. This $e^{-j\phi}$ excitation suppresses all of the even modes, as in the bifilar helix, and mode $e^{-j3\phi}$ as well. $e^{-j5\phi}$ is not suppressed. The bandwidth ap-

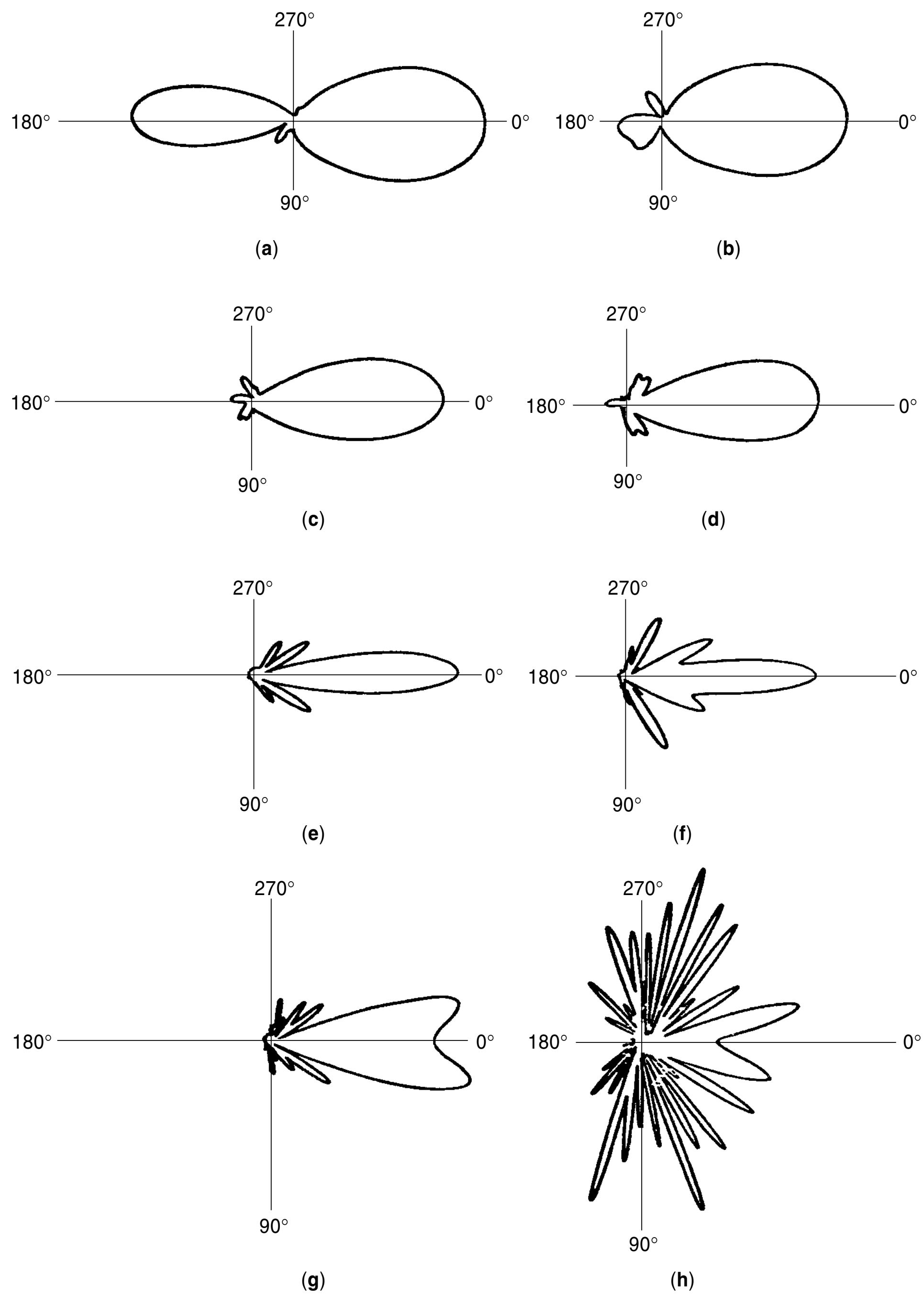

Figure 6. Beam patterns of the axial mode quadrifilar helix antenna. $C_\lambda = 0.44$, 0.52, 0.72, 1.1, 1.6, 1.8, 2.1, 2.7 in (a) through (h), respectively. From A. T. Adams and C. Lumjiak (17). © 1971 *IEEE*. Reprinted with permission of *IEEE*.

proaches 5 : 1. A pitch angle of approximately 40° is required. In general, with the M-filar helix, the mode $e^{-j\phi}$ is excited around the periphery. All other modes up to $e^{-jM\phi}$ are suppressed. The bandwidth lies between M and $M + 1:1$.

Gerst and Worden determined that the frequency range of the multifilar axial mode helix may be approximated as follows (15):

$$C_{\lambda\,\min} < C_\lambda < C_{\lambda\,\max} \tag{37a}$$

$$C_{\lambda\,\min} = \frac{\cos\alpha}{1+\sin\alpha} \tag{37b}$$

$C_{\lambda\,\max}$ is the lesser of $C_{\lambda\,\max 1}$ and $C_{\lambda\,\max 2}$:

$$C_{\lambda\,\max 1} = \frac{\cos\alpha}{1-\sin\alpha} \tag{37c}$$

$$C_{\lambda\,\max 2} = \frac{M}{2}\cot\alpha \tag{37d}$$

where M is the number of wires. Equation (37) can be used to predict the bandwidth of the axial mode unifilar or multifilar helix. For example, consider the monofilar helix with $\alpha = 14°$, whose beam patterns and other characteristics are given in Figs. 3 and 4. The figures indicate that the bandwidth is approximately $0.75 < C_\lambda < 1.25$ as noted previously. In comparison, Eq. (37) predicts that $C_{\lambda\min} = 0.78$ and $C_{\lambda\max} = 1.28$ for an approximate bandwidth of $0.78 < C_\lambda < 1.28$. The two bandwidth ratios are very close. Equation (37) has been applied to bifilar, quadrifilar, and octofilar axial beam helices, and the results agree well with experiments as shown in Refs. 15–17. Figure 6 shows the beam patterns of a quadrifilar helix antenna with a ground plane [see Fig. 5(a)]. The pitch angle α is 35°, diameter D is 3″, antenna length is 24″, ground plane diameter D_G is 10″, and the tape width is 1/2″. The feed system (16) provides four outputs that are phased 0°, 90°, 180°, and 270°, each output being connected to one of the four wires of the quadrifilar helix antenna. Equations (37b,c) yield $C_{\lambda\min} = 0.52$ and $C_{\lambda\max} = 1.92$ for $\alpha = 35°$ and $M = 4$. Thus the bandwidth of the antenna is given by $0.52 < C_\lambda < 1.92$ for a bandwidth ratio of 3.7 : 1. The progression of the beam patterns may be described as follows. At a frequency somewhat below the lower limit, backfire operation begins, as evidenced by the strong backlobe at $C_\lambda = 0.44$. The backlobe decreases rapidly as we approach the lower limit. The axial ratio also decreases rapidly and is less than 2 : 1 at the lower limit. Other antenna characteristics such as VSWR are also acceptable (17). The axial mode then predominates over the 3.5 : 1 bandwidth. The beam pattern narrows steadily and the directivity increases with frequency. The upper limit occurs at $C_\lambda = 1.92$, at a frequency just above that of Figure 6(f). Above the upper limit, beam-splitting occurs at $C_\lambda = 2.10$ and complete pattern breakup at $C_\lambda = 2.70$. Thus, with the multifilar helix, the bandwidth of the axial mode is extended to both lower and higher frequencies as predicted in Eq. (37).

The beam pattern at C_λ =1.80 exhibits the undesirable characteristic of high side lobes. This is caused by the backfire operation, which changes from backfire through sidefire towards endfire as frequency increases. It is sometimes called a "scanning" mode. The quadrifilar helix may also be used in a counterwound version with both right- and left-hand windings. The on-axis polarization is linear rather than circular. The backfire mode is much more effectively suppressed in this version, and the sidelobe levels are much lower. Bandwidths are between 4 : 1 and 5 : 1 as shown in (16). Gerst and Worden (15) describe a 53° pitch angle counterwound octofilar helix with 9 : 1 bandwidth. The multifilar helix antenna does not radiate in a normal mode at low frequencies because of the phase excitation 0°, 90°, 180°, and 270° of the windings. The excitation $e^{-j\phi}$ is a supergain excitation at low frequencies ($C_\lambda \ll 1$). Details on the axial multifilar antenna are given in (15–17) and related references.

The Backfire Quadrifilar Helix

In the analysis of circular loops we noted that, with $e^{\pm j\phi}$, circularly polarized radiation occurs at both $\theta = 0, 180°$. To distinguish between these two directions, we need additional information about the helix. A rigorous analysis of the infinite monofilar helix by Paul Klock (14) shows that there are two modes operating simultaneously in the axial mode region. Both involve $e^{-j\phi}$ excitation for right-hand helices and are circularly polarized on axis. One is the axial mode and the other is a *backfire* mode which starts at backfire and scans forward as a conical beam as frequency increases. We may, for purposes of discussion, combine the backfire and forward-scanned operations into a single backfire designation. In the mono- and quadrifilar helix the backfire mode shows up just before the onset of the axial mode. The backfire mode exists along with the axial mode, but is suppressed by the presence of the ground plane. The backfire mode is *favored* over the forward endfire as pitch angle increases. Pitch angles in the 40–50° range with no ground plane show both forward and backward radiation. With no ground plane, the radiation is primarily backfire. For the right-hand helices of Figs. 1 and 5, the endfire radiation is right-handed circularly polarized and the backfire radiation is left-handed circularly polarized.

The backfire bifilar helix was first studied by Patton (18), who carried out extensive theoretical and experimental work. He showed the range of backfire beam patterns which were obtained with the monofilar and bifilar helices. Later, Charles Kilgus (19) showed that beam pattern improvements could be obtained with the quadrifilar helix. He investigated in detail the shaped-conical and cardioid patterns which are obtainable with the backfire quadrifilar helix.

Figure 5(b) shows the backfire quadrifilar helix. It consists of two bifilar antennas fed 90° out of phase to produce the $e^{-j\phi}$ excitation. No ground plane is required and the ends of the helices may be shorted together. The backfire helix is used with pitch angles as high as 60° and 70°. With these high pitch angles, the backfire mode can operate at low frequencies, yielding a small cross section for the antenna.

A typical shaped conical beam is shown in Fig. 7. The beam is very wide for broad sector coverage with a dip or a local maximum (not shown) at the center ($\theta = 180°$). The dip is appropriate for satellite coverage, because it can be chosen to yield uniform signal strength at the receiver as the satellite passes. Kilgus (19) shows numerous beam patterns for different designs. The beamwidths vary from 100 to 180°. Directivities of up to 7 dB are observed.

The backfire quadrifilar helix has characteristics that make it especially suitable for many satellite, spacecraft, and navigational applications. It has been used as a transmitter and receiver in satellite communication systems and as a receiver for GPS applications (20). It has also been considered for cellular phones and new GPS applications (21).

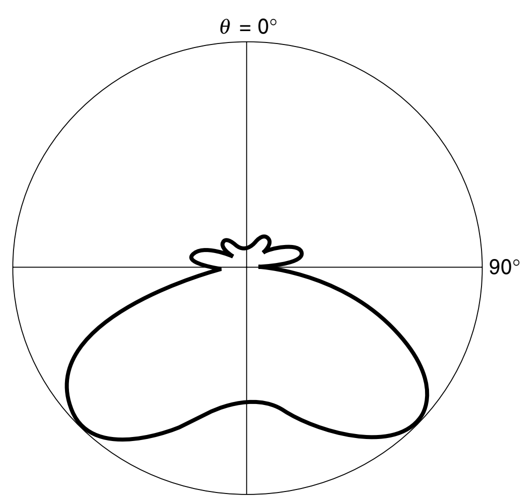

Figure 7. Beam pattern of the backfire quadrifilar helix.

SUMMARY

The helical antenna, first discovered in 1946 by John Kraus, has evolved into many different forms with many different applications. The normal mode helix has some advantages for low-frequency applications. The broadband, circularly polarized, axial mode helix radiates forward endfire along its axis. It has been the most widely used of all forms of the helix. The quadrifilar axial mode helix extends the bandwidth further. The backfire quadrifilar helix radiates a broad sector coverage suitable for satellite applications.

BIBLIOGRAPHY

1. J. D. Kraus, *Antennas,* 2nd ed., New York: McGraw-Hill, 1988, pp. 265–339.
2. W. L. Stutzman and G. A. Thiele, *Antenna Theory and Design,* 2nd ed., New York: Wiley, 1998, pp. 231–239.
3. W. W. Hansen and J. R. Woodyard, A new principle in directional antenna design, *IRE Proc.,* **26**: 333–345, 1938.
4. C. A. Balanis, *Antenna Theory: Analysis and Design,* 2nd ed., New York: Wiley, 1997, pp. 271–276.
5. H. Nakano, *Helical and Spiral Antennas: A Numerical Approach,* New York: John Wiley and Sons, 1987, pp. 123–195.
6. R. S. Elliott, *Antenna Theory and Design,* Englewood Cliffs, NJ: Prentice-Hall, 1981, pp. 71–78.
7. H. E. King and J. L. Wong, Characteristics of 1 to 8 wavelength uniform helical antennas, *IEEE Trans. Antennas Propagat.,* **AP–28**: 291–296, 1980.
8. E. A. Wolf, *Antenna Analysis,* New York: Wiley, 1967, pp. 437–444.
9. R. C. Johnson and H. Jasik, *Antenna Engineering Handbook,* 2nd ed. New York: McGraw-Hill, 1984, pp. 13-1–13-23.
10. J. L. Wong and H. E. King, Broadband quasi-taper helical antennas. *IEEE Trans. Antennas Propagat.,* **AP-27**: 72–78, 1979.
11. L. O. Krause, Sidefire helix UHF-TV transmitting antenna, *Electronics,* **24**: 107–109, Aug. 1951.
12. J. D. Kraus, *Radio Astronomy,* 2nd ed., Powell, OH: Cygnus-Quasar, 1986.
13. S. Sensiper, Electromagnetic wave propagation on helical structures, *Proc. IRE,* **43**: 149–161, 1955; also Ph.D. Thesis, M.I.T., 1951.
14. P. W. Klock, *A Study of Wave Propagation of Helices,* Ph.D. Thesis, University of Illinois, Urbana-Champaign, 1963.
15. C. Gerst and R. A. Worden, Helix antennas take turn for better, *Electronics,* **39**: 100–110, Aug. 1966.
16. A. T. Adams et al., The quadrifilar helix antenna, *IEEE Trans. Antennas Propagat.,* **AP-22**: 173–178, 1974.
17. A. T. Adams and C. Lumjiak, Optimization of the quadrifilar helix antenna, *IEEE Trans. Antennas Propagat.,* **AP-19**: 547–548, 1971.
18. W. T. Patton, *The Backfire Helical Antenna,* Ph.D. Thesis, University of Illinois, Urbana-Champaign, 1963.
19. C. C. Kilgus, Shaped-conical radiation pattern performance of the backfire quadrifilar helix, *IEEE Trans. Antennas Propagat.,* **AP-23**: 392–397, 1975.
20. J. M. Tranquilla and S. R. Best, A study of the quadrifilar helix antenna for global positioning system (GPS) applications, *IEEE Trans. Antennas Propagat.,* **AP-38**: 1545–1550, 1990.
21. N. Padros et al., Comparative study of high-performance GPS receiving antenna designs. *IEEE Trans. Antennas Propagat.,* **AP-45**: 698–706, 1997.

ARLON T. ADAMS
JAY K. LEE
Syracuse University